ASCE

# Probabilistic Resilience Measurement for Rural Electric Distribution System Affected by Hurricane Events

Prativa Sharma, S.M.ASCE[1]; and ZhiQiang Chen, M.ASCE[2]



**Abstract:** This paper proposes a fully probabilistic and analytical measurement framework for assessing the resilience of linear power-distribution systems affected by hurricane wind. The topology of rural power-distribution systems can be largely characterized as a set of linear subsystems that emanate from one power substation and individually feature zero redundancy. Moreover, rural power-distribution systems are less robust owing to their high vulnerability to material aging, and they demand longer recovery times due to low socioeconomic resources in rural areas. The proposed framework includes a mechanical analysis of a coupled wood pole and feeder line as a system unit, a definition of component restoration and system-level recovery functions, and, finally, a definition of a new resilience measure, referred to as total mean system resilience (TMSR). Numerical experimentation is provided that validates the effectiveness and analytical tractability of the framework. Insight into how physical aging, local resourcefulness, and spatial sparseness interplay and affect the system resilience is given quantitatively in this paper. **DOI: 10.1061/AJRUA6.0001061.** © *2020 American Society of Civil Engineers.*

**Author keywords:** Power distribution; Resilience; Vulnerability; Rural; Hurricane; Resourcefulness; Aging.

## Introduction

Electricity infrastructure, including power-transmission and power-distribution systems, are of paramount importance in all civil infrastructure systems (CISs) because electricity is the most universal and direct energy source for supporting other CISs (DHS 2011). Among different types of climatic events that cause power outages, coastal hurricanes and tropic storms are reportedly the major causes in the United States from 1984 to 2012 (Kenward and Raja 2014). In particular, the deadliest hurricane landfalls have triggered an average economic loss of $25 to $70 billion annually due to power outages (Vugrin et al. 2017). These soaring losses may hide a striking fact—although the economic losses concentrate in densely populated urban centers, the postdisaster recovery in rural areas is much slower than that in urban centers. A prominent example is recovery from power outages, which may last from a few hours in urban areas to weeks and sometimes months in rural areas. An example of such outages is Puerto Rico, where the power outage in the rural village of Adjuntas lasted for almost a year in the aftermath of Hurricane Maria in September 2017 (Danica Coto 2018). Adopting the notion of resilience in the context of civil infrastructure engineering, which is the ability to prepare for, withstand, and recover from disruptions (Ayyub 2014; Cimellaro et al. 2010), this obviously signifies the low resilience of power systems in these rural areas. In this paper, the authors identify three intrinsic indicators that account for the low *resilience* of rural power systems:

1. *Material aging*. One report indicates that among the six largest utility companies in the US, the percentage of wood distribution poles with service ages exceeding 40 years ranges from 15% to 50%, and the percentage of those exceeding 60 years old reaches as high as 5%–15% (Brown and Willis 2006). Wood poles are susceptible to aging due to fungal decay and other environmentally related deterioration (Morrell 2012). These poles after serving for years often suffer from a significant loss of structural capacity against wind loads, which statistically results in low system reliability. On the other hand, wood poles are much more widely used in rural distribution systems than in urban areas. One FEMA hurricane report suggested the replacement of wood poles with concrete or metal poles after observing the significant losses of utility structures, but it also indicated that rural electric cooperatives are likely to continue the use of wood poles (Burbank et al. 2005).
2. *Low redundancy*. In urban areas, infrastructure systems are mostly in networks that include connected substations, transmission, distribution systems, and power switches. In such a networked system, redundancy is essential and enforced. As such, any failure in a confined area can be isolated and the remaining system continues to function (Dueñas-Osorio et al. 2007; Reed et al. 2009). Comparatively, power systems in rural areas usually feature a pattern of linear distributions, which emanate from a central substation and then pass through service areas without alternative connections to other substations or power sources. In fact, such a linear power-delivery subsystem has zero redundancy; even with more than one substation servicing the same area, the redundancy remains at a very low level.
3. *Low resourcefulness*. The third indicator lies in the social/economic dimensions measured by local resourcefulness. In urban areas, local resources (including trained personnel, vehicle support, safety support, and use of technologies) are relatively abundant. This abundance of resources directly determines the rapidity of recovery or rate of recovery. In contrast, lower resourcefulness in disaster preparation and response is a signature of most rural areas, and rural communities increasingly find themselves short of resources in dealing with climate change and hazards (Brennan and Flint 2007; Kapucu et al. 2013).

[1]Ph.D. Candidate, Dept. of Civil and Mechanical Engineering, Univ. of Missouri Kansas City, FH 5110 Rockhill Rd., Kansas City, MO 64110. Email: pswzg@mail.umkc.edu

[2]Associate Professor, Dept. of Civil and Mechanical Engineering, Univ. of Missouri Kansas City, FH 5110 Rockhill Rd., Kansas City, MO 64110 (corresponding author). ORCID: https://orcid.org/0000-0002-0793-0089. Email: chenzhiq@umkc.edu

Note. This manuscript was submitted on June 20, 2019; approved on December 6, 2019; published online on March 31, 2020. Discussion period open until August 31, 2020; separate discussions must be submitted for individual papers. This paper is part of the ***ASCE-ASME Journal of Risk and Uncertainty in Engineering Systems, Part A: Civil Engineering***, © ASCE, ISSN 2376-7642.

Resourcefulness is dynamic, not only as socioeconomic conditions improve or worsen over time but also when distributions of interconnected infrastructure systems change spatially. In urban areas, the physical and social infrastructure systems are closely distributed, whereas in rural areas, they are geospatially sparse. Very little research has been conducted on the relation of resources (e.g., technologies) and geospatial sparseness of infrastructure. A recent study proposes a general framework for bridging the digital divide in rural preparedness and response for emergencies, which in particular mentions the factor of geospatial sparseness in connection with civil infrastructure and population in rural areas (Gascó-Hernandez et al. 2019). As a result of this geospatial sparseness, the aforementioned weak resourcefulness in rural areas is further exacerbated and should be coupled with geospatial factors.

Given these three factors, one may understand that recovery from a power outage in rural areas can take an inordinate amount of time. It should be noted that from a structural and infrastructural engineering point of view, it is straightforward to understand the physical effects of aging and a system's low-redundancy factor, which together lead to enhanced likelihood of system failure and, hence, greater losses (or less system robustness). Nonetheless, existing knowledge in this engineering domain is does not allow for measuring the effects of local resourcefulness that local communities and stakeholders can deploy in the aftermath of extreme events. Observation-based evidence manifesting a higher level of resourcefulness was seen from the recovery effort for Hurricane Harvey, which made landfall in August 2017 in Texas. In the aftermath of this event, 96% of affected customers (ACs) saw power restored within 2 weeks of the event (Britt 2017). The Center Point Energy Houston Electric (CEH) pointed out that the use of advanced meters, intelligent grids, all-terrain vehicles (ATVs), drones, and helicopter-based remote sensing has helped to shorten outages (Britt 2017). The two resilience examples (including that of Puerto Rico discussed earlier) reveal that for a similar type of infrastructure, *resilience disparity* is evident and real owing to the different degrees of resourcefulness in urban and rural areas.

Because the first step in fully understanding and assessing rural power-system resilience, this paper aims to develop an analytical framework for quantifying the linear power-delivery subsystems typically found in rural power systems. The framework includes a mechanical analysis of a coupled wood pole and feeder line as a system unit, a definition of component restoration and system-level recovery functions, and, finally, a definition of a new resilience measure, referred to as total mean system resilience (TMSR). When formulating the component-based restoration and system-level recovery functions, the innovation in the approach also lies in the fact that both resourcefulness and spatial-sparseness parameters are parametrically integrated into the framework.

## Related Work

### Resilience Quantification

The notion of resilience measurement has been classically illustrated as a piecewise function model with the phases of performance or functionality degrading, dropping, and recovering (e.g., Bilal 2015; Cimellaro et al. 2010). In Fig. 1, the pre-event performance is assumed to be a constant at a perfect (100%) functionality level; in practical terms, the system degrades slowly by developing aging-induced degradation or incidentally due to minor or moderate-level hazards. Following the leading definitions when measuring resilience, as illustrated in Fig. 1, $t_{oe}$ is the time of the event, $t_{re}$ is the time for the entire system to fully recover, and $t_c$ is the control time or the planning horizon to calculate the resilience of the system (Bilal 2015; Cimellaro et al. 2010). The control time ($t_c$) can be set per judgment depending on the type of structural system or simply set as the return period of the hazard of interest. For example, the control period for power distribution/transmission in urban areas,

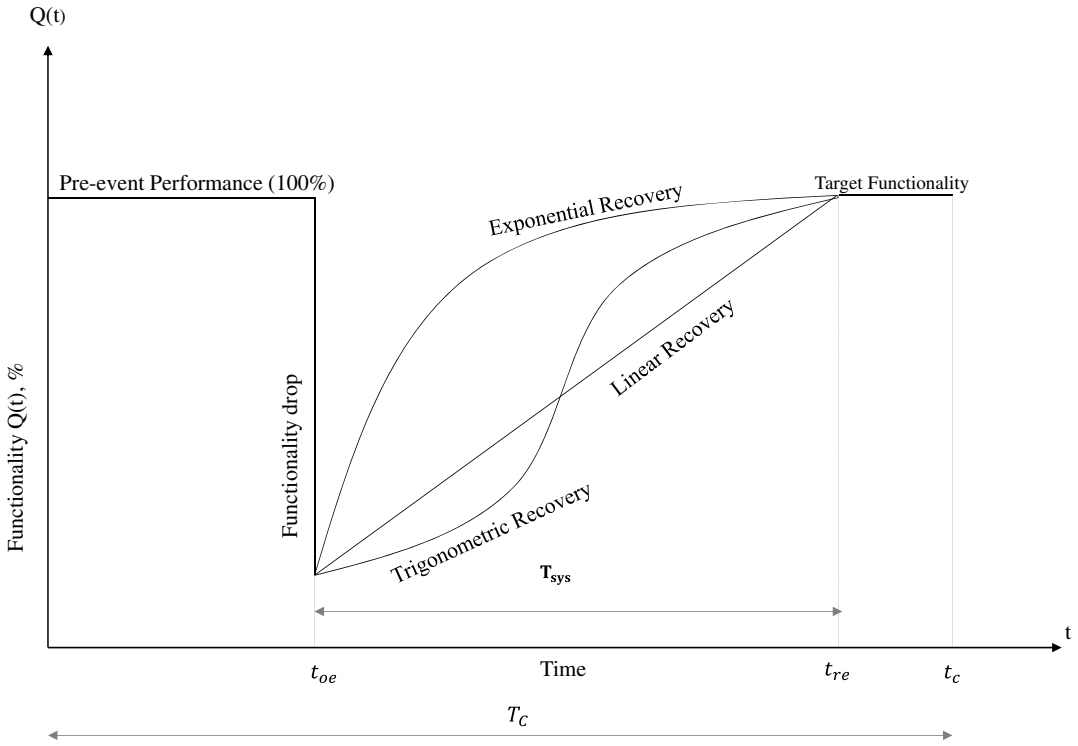


**Fig. 1.** Graphical illustration of resilience measurement.



ASCE-ASME J. Risk Uncertainty Eng. Syst., Part A: Civ. Eng., 2020, 6(2): 04020021

clustered with residences, industries, and lifeline infrastructure systems, should be less than an hour; an hour of downtime can cause significant monetary damage or loss of life. However, the control time ($t_c$) as evidenced in past events in rural areas can last months or more than a year. The key element to calculate the resilience is the system recovery function, which connects the decreased level of functionality and the recovered functionality as of time.

Different types of recovery functions, featuring different recovery rates that are the first-order derivatives of the recovery functions, have been introduced by Cimellaro et al. (2010). The selection of a system recovery function is largely empirical based on the availability of information about the intrinsic properties of the given structures, the robustness of the system, and the socioeconomic resources available to stakeholders (Cimellaro et al. 2010).

The mathematical definition of resilience used in this paper is the one described by Ayyub (Bilal 2015). Briefly, resilience ($R_{sys}$) is defined as the normalized area underneath the system recovery function within the interval of the functionality-drop time and the defined control period ($T_C$), as shown in Fig. 1. Analytically, Ayyub's resilience equation is

$$R_{sys} = \frac{\int_{t_{oe}}^{t_{re}} f_{rec}(t)\mathrm{dt} + (T_C - \mathrm{T_{sys}})Q_{100}}{T_C \times Q_{100}} \tag{1}$$

where $f_{rec}(t)$ = system recovery function; $Tc$ = control period; $\mathrm{T_{sys}}$ = time required for the system to recover after the strike; and $Q_{100}$ = performance measurement when the system is fully functional before the strike.

### Resilience Assessment for Power-Delivery Systems

A number of efforts are made to focus on system performance assessment for power-delivery (transmission or distribution) infrastructure subject to extreme weather or terrorist attacks. Panteli and Mancarella used a sequential Monte Carlo simulation to model weather-related fragility models for transmission towers and further assessed the resilience of power systems (Panteli and Mancarella 2017). This fragility model was used by Espinoza et al. (2016) as one of the phases to assess the resilience of transmission networks calculating the expected energy-not-supplied (EENS) resilience index and the energy index of unreliability (EIU) when subjected to extreme events and flooding (Espinoza et al. 2016; Panteli et al. 2017). Some studies have identified the most critical line in a transmission network that could cause the maximum outage and proposed to harden the same transmission line for improved resilience (Bier et al. 2007; Yao et al. 2007). Historical data of power outages have been explored in several studies to come up with estimated power outage during extreme events. For instance, Davidson et al. (2003) investigated the performance of the electric distribution system subject to hurricanes based on historical data of outage hours, geographical distributions, and causes of outages. Guikema and Goffelt (2008) assessed the reliability of power-delivery systems using regression analysis that was useful for underdispersed and overdispersed outages. Liu et al. (2005) used a negative binomial regression model based on geographic information system (GIS) database of outages to predict the number of outages likely to occur in each square kilometer of grid cell of the specified region. Zhu et al. (2007) created empirical models using historical outage data and used those models to predict outages in real-time storms. Although these models are found to be effective at predicting outages due to single hurricane events, acquiring accurate historical data could be the problem. On the other hand, addressing the network topology or performance of each component of the electric system is very important, but such a concern appears to be lacking in these studies.

A limited number of research endeavors concern the resilience of power-delivery systems, and much fewer address power systems in rural areas. Ouyang and Dueñas-Osorio developed a probabilistic model considering the complex power-delivery networks including nodes representing generators, substations, and load points and edges as either transmission or distribution lines (Ouyang and Dueñas-Osorio 2014). Given the complexity of the system, simplified vulnerability modeling in terms of damage functions or fragility models were used for the system components. A fragility study of a three-span pole-wire system of a power-distribution network subjected to strong wind was conducted to determine the hardening of poles and inspection priorities (Yuan et al. 2018). Kwasinski proposed metrics for resilience assessment and verified the interrelation between resilience, resistance, and brittleness for power grids (Kwasinski 2016). Some researchers emphasized the concept of microgrids and resource allocation for enhancing the resilience of distribution networks (Chen et al. 2016; Gao et al. 2016; Li et al. 2014).

To this end, several research gaps are recognized considering the efforts just reviewed. First, there is no framework that systematically accounts for system robustness, redundancy, and resourcefulness collectively for power-delivery systems. Second, regardless of rural or urban power systems, empirical functions are often used without a mechanical (or first-principle) basis when computing system reliability or vulnerability. Third and lastly, rural power-delivery systems are rarely treated in the literature in connection with quantitative resilience assessment.

## Analytical Framework

### Model Idealization and Methodology Framework

Most distribution networks in rural areas operate in a linear configuration and can be represented as a minimum spanning tree (Warwick and Hoffman 2016). Fig. 2(a) presents an illustrative example, where a "leaf" is recognizable when a substation is selected. Taking advantage of this topological characteristic and without losing the generality, this paper considers a generic "leaf" as the object of interest, as shown in Fig. 2(b). This leaf-like power-delivery subsystem is assumed to have $N$ poles and $N$ conductor cable segments (counting from the end to the substation, $i = 1, 2, \ldots, N$). This linear power-delivery subsystem is henceforth referred to as a *system* for the sake of simplicity in this paper. Given this linear conductor-pole system, any failure of an upstream feeder line or pole will cause an outage to all the downstream customers (Davidson et al. 2003). Assuming that for the $i$th pole it individually feeds the power to $Nc_i$ customers, the total number of customers served by this power delivery system is $\sum_{i=1}^{N} N_{c_i}$. Note that the failure of substations, transmission towers, and other electrical components, as typically encountered in urban-area power infrastructures, is outside the scope of this study.

With this general rural power-delivery system, a probabilistic resilience measurement framework is proposed in this paper. This framework has four sequential steps, described as follows:

1. *Probabilistic system vulnerability modeling*. This step produces the failure probability given a hurricane event characterized by its hurricane category ($H$). Mechanical analysis based on the material properties of wood poles and feeder conductors of the system is the core element of this step. Two reduced-order analysis methods are adopted, including the analytical cable method and the empirical pole-capacity model in this paper, which yield the conditional failure probability distributions for a generic pole and a conductor.

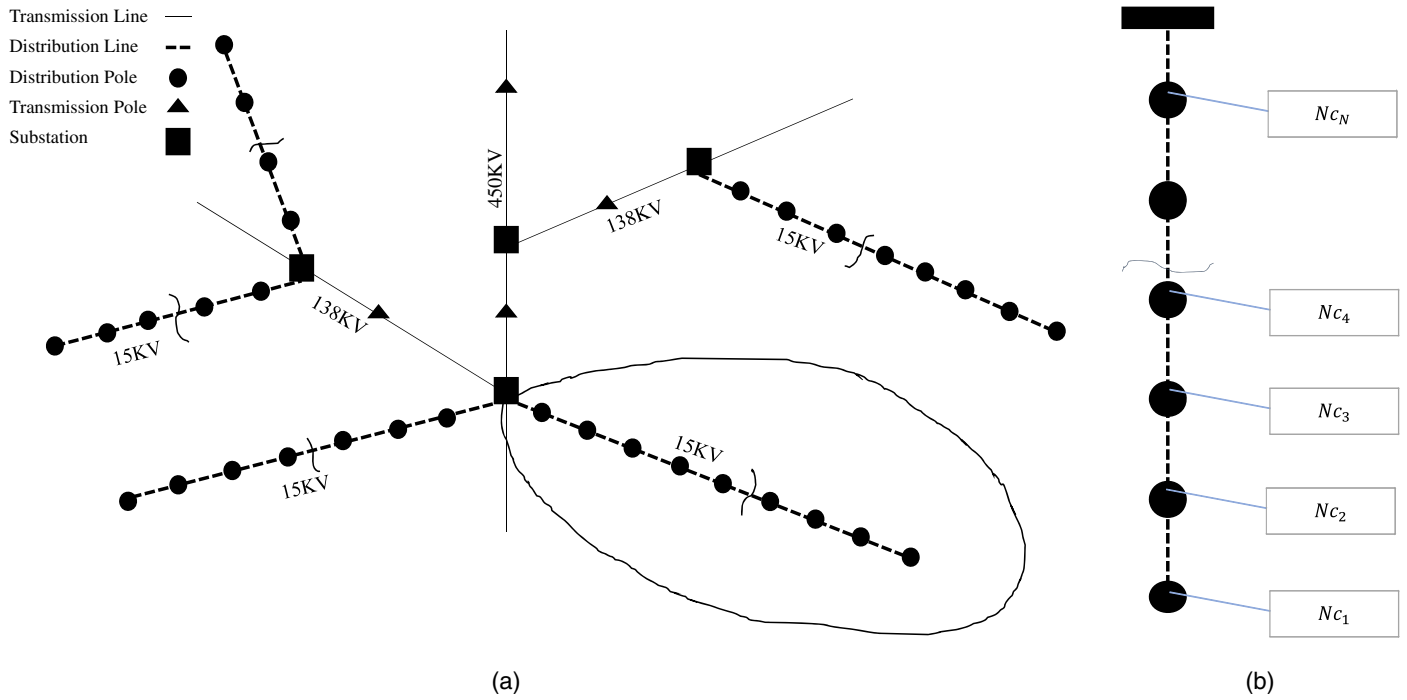


**Fig. 2.** (a) Typical rural power-distribution configuration; and (b) a single span with N poles in a radial subsystem.

2. *Probabilistic system functionality modeling*. The probabilistic system functionality model incorporates the structural-system vulnerability model and the notion of loss in the power-delivery system. In this work, the functionality loss is characterized in terms of the number of customers collectively summed up due to the failure event, upon which the discrete probability mass function (PMF) for the system function is defined.
3. *Probabilistic system recovery modeling*. To quantify system recovery and measure resilience, local resourcefulness and geographical sparseness are crucial parameters that govern system recovery. In this paper, a novel and general component-level restoration model is proposed, which is then used to formulate the system-level restoration time and the system recovery function.
4. *Probabilistic resilience modeling*. This final step measures the resilience of the system as described in Eq. (1), where the recovery function is integrated mathematically (leading to an area calculation, essentially). The final resilience measure is formulated probabilistically, which leads to the definition of TMSR.

## Probabilistic System Vulnerability Modeling

### Order-Reduced Conductor-Pole Model

To assess the vulnerability of poles and cables, ideally, a mechanics-based structural model is required. The widely adopted solution is a finite-element (FE)–based modeling of the complete and connected system of poles and conductors, where multiple poles with multiple spans of sagged cables with the proper material and element models are subjected to the wind loads of select intensity levels (Pang et al. 2013). However, such a model would be computationally prohibitive when conducting a stochastic simulation. As will be shown later, the probability of failure for a conductor or a pole is as small as can be stochastically sampled; the system-level probability of failure in many scenarios can be extremely small and, hence, not manageable if a sampling approach is used. In this work, an order-reduced model with a single span of a sagged cable pinned at two nodes is adopted, as shown in Fig. 3(b). This model, fully solvable analytically (Impollonia et al. 2011), can account for the geometric nonlinearity of the cable and the elasticity of the supports. Considering uniformly distributed wind loads (with a variable wind direction angle in three dimensions) and the self-weight load of the cable, the tension in the cable can be expressed as

$$\mathbf{T}(\ell) = \mathbf{R}_0 - \mathbf{P}\ell \tag{2}$$

where $\mathbf{R_0} = [Rx, Ry, Rz]$ = reaction force vector at origin (left-end support); $\mathbf{P} = p\boldsymbol{\pi}$ = vector of a distributed load with an intensity $p$ acting along the cable in the direction defined by a vector $\boldsymbol{\pi}$; and $\mathbf{T}$ = cable tension vector as a function of the Lagrangian coordinate $l$ that represents a unit length of the unstrained cable. The wind speed and direction are chosen as the major load parameters. However, note that heavy rainfalls accompanying a hurricane landfall and the ensuing flooding may also contribute to the structural failure. In this paper, the effects of flooding or rainfalls are not included in the framework. If one desired to include these effects, the mechanical model subject to these hazards needs to be considered, leading to different failure probabilities of poles and conductors. For solving Eq. (2), the closed-form solution is derived at the position $l$ satisfying a stretched configuration, which is expressed by Eq. (3):

$$\boldsymbol{\varepsilon}(s) = C\left(\mathbf{r}s - \boldsymbol{\pi}\frac{s^2}{2}\right) + (I - \boldsymbol{\pi}\boldsymbol{\pi}^{\mathrm{T}})r \times \ln\left[\frac{\rho(\boldsymbol{\pi}s)}{\rho(0)}\right] - \boldsymbol{\pi}(\|\mathbf{r} - \boldsymbol{\pi}s\| - \|\mathbf{r}\|) + \boldsymbol{\varepsilon}(\mathbf{0}) \tag{3}$$

where $\boldsymbol{\varepsilon}(s)$ = dimensionless position vector; $C = (pL)/(EA)$ ($L$ = unstrained cable length; and $E$ and $A$ = Young's modulus and area of cable section, respectively); $\mathbf{r}$ = dimensionless reaction force at cable origin; $s$ = dimensionless coordinate of $l$; and $\rho(\cdot)$ = operator performing $\rho(\cdot) = \|\mathbf{r} - \cdot\| - \boldsymbol{\pi}^T[\mathbf{r} - (\cdot)]$. The detailed formulation for Eqs. (2) and (3) are found in Impollonia et al. (2011).

A verification study using the FE- based multispan model as seen in Fig. 3(a) is found in Pang et al. (2013), which shows sufficient accuracy when comparing the nonlinear behavior of a midspan cable of the three-dimensional (3D) model against the reduced-order model.

Furthermore, the resultant reaction, namely $\mathbf{R_0}$ defined in Eq. (2), is applied to the pole structure as the wind-induced force demand unto the poles. This contributes to the bending moment and shear demands made on the pole structures, which are in general maximal at the base of the poles. In addition to this demand coming from the conductors, the wind on the vertical profile of the poles contributes to the base moment and shear-force demands as well. Thus, the two sources of bending moment demands at the ground line of the pole ($M_B$) are combined and then compared with the bending capacity ($S$). That is, if $M_B > S$, a failure event occurs. For treated wood poles, the following equation, recommended by the ASCE report "Reliability-Based Design of Utility Pole Structures," is adopted to define the bending capacity (Dagher 2006):

$$S = 0.0098 \times F_b \times C_g^3 \tag{4}$$

where $F_b$ = fiber stress in MPa for the type of wood considered; and $C_g$ = ground-line circumference of pole in inches, and the resulting $S$ has a unit in kN-m. Untreated wood poles are more prone to aging because material decay reduces the strength capacity of poles (Wang et al. 2008). The bending capacity $S$ after considering aging is calculated as

$$S = 0.0098 \times F_b \times [C_g - \pi d(t)]^3 \tag{5}$$

where $d(t)$ = decay depth at a time $t$ (year), which depends on rate of decay (defined as $r = k_{\text{wood}} k_{\text{climate}}$, where the $k$ parameters relate to the type of wood and the climate of the region being considered). The detailed procedure to calculate $d(t)$ is found in Wang et al. (2008).

### Stochastic Estimation of Failure Probabilities

The random variables used in this study are the wind speed, wind direction for the desired hurricane category, the fiber strength of timber for the pole, and the tensile strength of the cable material. These random variables are treated probabilistically independent, and Table 1 lists the distribution types and parameters for the involved variables in this work. Specifically, the lognormal distribution was considered as a proper statistical distribution for modeling random material-strength variables (Sakai et al. 1997; Torrent 1978), including the rated fiber strength ($F_b$) of timber and the tensile strength of the feeder-line conductors ($F_y$). The mean value for the fiber strength for common wood species for poles can be obtained from ANSI (2017). The mean value for the tensile strength of solid/stranded bare copper wires and cables can be obtained from standards and specifications available (e.g., Southwire 2013). The standard deviations for these material properties depend on the quality of the given manufacturers and other operational factors. In this paper, 1% of the mean value is taken as the standard deviation for the distributions.

For hurricane winds, however, a Weibull distribution with a shape parameter of 2 matches fairly well the wind distribution for inconsistent wind with high speed (Archer and Jacobson 2003; Edwards and Hurst 2001), so it is used in this paper to model the wind pressure for a given hurricane category. For the site-specific case, users can estimate the distribution parameters and perform a goodness-of-fit test to check the adequacy of the distribution model to the recorded wind speed data. In the literature, Gumbel Type I distributions have been adopted for modeling the distribution of hurricane wind speed (Carlos Agustín 2013; Vivekanandan 2012). Users can select these distributions while adopting the proposed framework. By adopting the Weibull distribution, the mean wind speed at a hurricane category $H$ is determined based on the Saffir–Simpson Hurricane Wind Scale (SSHWS), and the scale parameter of the Weibull distribution is calculated as indicated in Table 1. To consider the randomness in wind direction, a random direction vector in the $x$-$y$ plane is considered. Denoting the relative angle to $x$ by $\theta$, which follows a uniform distribution in the range $[0, \pi]$, the random direction of the wind in 3D coordinates is expressed as a vector of $[\text{Cos}(\theta), \text{Sin}(\theta), 0]$.

Based on the closed-form solution as shown in Eq. (3), which shows the analytical solution for a cable in three dimensions subject to a uniform force vector in a designated direction, a first-order or second-order approximation method can be used to estimate the failure probability of the cable. Nonetheless, the sampling technique provides a more straightforward and efficient solution without using any analytical approximation. In this paper, the Latin hypercube sampling (LHS) method is selected because of its more convergent

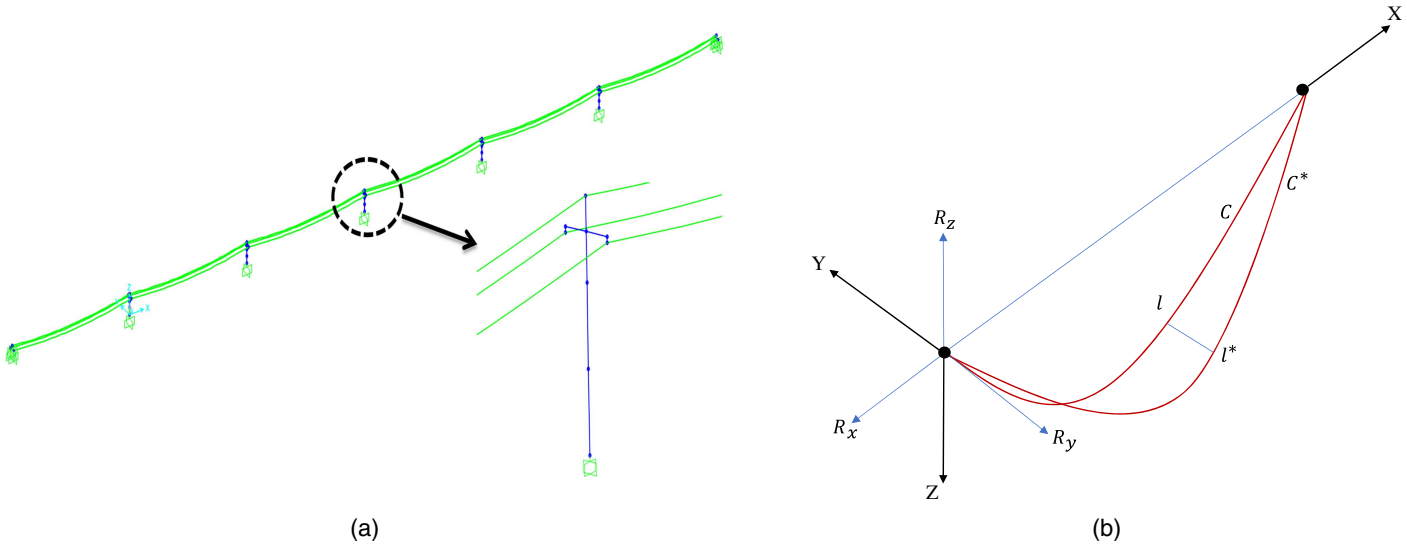


**Fig. 3.** (a) Finite-element model of a six-span power-delivery system; and (b) single-span configuration.

**Table 1.** List of distribution types and distribution parameters

| Variable | Distribution | Parameter | |
|---|---|---|---|
| Fiber strength (Fb) | Lognormal | 55.16 MPa (8,000 psi) (mean) | 8.27 Mpa (1,200 psi) (standard deviation) |
| Tensile strength (Fc) | Lognormal | 28.7 kN (6,453 lbf) (mean) | 2.87 kN (645.3 lbf) (standard deviation) |
| Wind speed | Weibull | 2 ($k$, shape parameter) | $\lambda$ (scale parameter)[a] |
| Wind direction | Uniform | 0°–180° (range) | |

[a]$\lambda$ = calculated using $\mu = \lambda\Gamma(1 + 1/k)$ given a value of $k$, where $\mu$ = mean wind speed based on Saffir–Simpson hurricane wind scale for a selected hurricane category.



property than a basic Monte Carlo method in approximating the distribution means and other higher-order moments of the random variables (Bilal and Lai 1990).

With Eqs. (3)–(5) and the LHS sampling technique, the response surface of the failure events for the two generic components are estimated based on the following definitions:

- $P_w = P(S\text{–}M_B < 0|H)$
- $P_c = P(F_y - T(\ell) < 0|H, G)$

where the two limit states $F_y - T(\ell) < 0$ and $S\text{–}M_B < 0$ define the failure events for the wood pole and the feeder conductor, respectively, and $P_c$ and $P_w$ are the conditional failure probability of the feeder conductor and the wood poles, respectively. Figs. 4(a and b) show the sampled response surfaces for the conductors (subject to wind speed and direction) and the pole (subject to wind speed, direction, and aging), both considering a hurricane category $H$ of III. With this sample response surface, the failure probability is estimated as the frequency that corresponds to the percentage of the failure events over the total sampling size as $P(\text{failure}) \cong$ (No. of failed sampled points)/(No. of total simulation samples). The failure criterion at a sampled point is determined based on the limit-state definitions: $F_y - T(\ell) < 0$ and $S\text{–}M_B < 0$. From the sampled response surfaces, the failure probabilities are calculated as 9% for the cable, 18% for the nonaged pole, and 41% for the 60-year-old pole, respectively.

Note that to consider the effect of aging, the aging factor is treated not as a random variable but as a deterministic condition in order to directly evaluate its effects on resilience measurement. Second, the conditional failure probabilities are calculated for a set of different hurricane categories at the select location. In the latter phase of the modeling, for the sake of simplicity, the variables $P_c$ and $P_w$ are used in the formulation without expressing the conditional variables (hurricane category $H$ and aging factor $G$). Further, note that if the fragility model for poles and conductors exists as a function of the wind speed ($V_w$), i.e., $P(S\text{–}M_B < 0|V_w, H)$ and $P_c = P(F_y - T(\ell) < 0|V_w, H, G)$, one can directly estimate the probability of failure by integrating out $V_w$ given its distribution to obtain $P_w$ and $P_c$, respectively.

### Probabilistic System Functionality Modeling

The system considered in this study has cascading effects such as a single failure of an upstream distribution feeder line, where either a conductor or a pole causes power outage to all customers downstream. Therefore, a natural function measure is the number of customers affected by the outage resulting from a failure event. Given a hurricane category $H$ and an aging factor $G$, considering $N$ poles (and $N$ conductor lines) from the linear power-delivery system, and that at the $i$th conductor-pole unit the number of customers served is $Nc_i$ ($i = 1$ to $N$), the sample space ($\mathcal{A}$) of the ACs considering all failure events is defined by Eq. (6):

$$\mathcal{A} = \left\{0, \sum_{i=1}^{1} Nc_i, \sum_{i=1}^{2} Nc_i, \sum_{i=1}^{3} Nc_i, \ldots\ldots\ldots \sum_{i=1}^{N} Nc_i\right\} \quad (6)$$

where a total of $N + 1$ different events, each of which is associated with a specific AC value, are defined. For the sake of simplicity, these AC events are redefined as $\mathcal{A} = \{A_m | m = 0, 1, \ldots, N\}$, where except that $A_0 = 0$, $A_m = \sum_{i=1}^{m} Nc_i (m = 1, 2, \ldots, N)$.

It is obvious that the maximum ACs ($A_N$) also defines the total number of customers that the linear power-delivery system serves. In this paper, this quantity is treated as a proxy to define the 100% functionality of the system, denoted by $Q_{100}$. Given a hurricane event, if $A_m$ ($A_m \in \mathcal{A}$) customers are affected, then the functionality drop is $A_m$, and the remaining number of customers ($Q_{100}$–$A_m$)

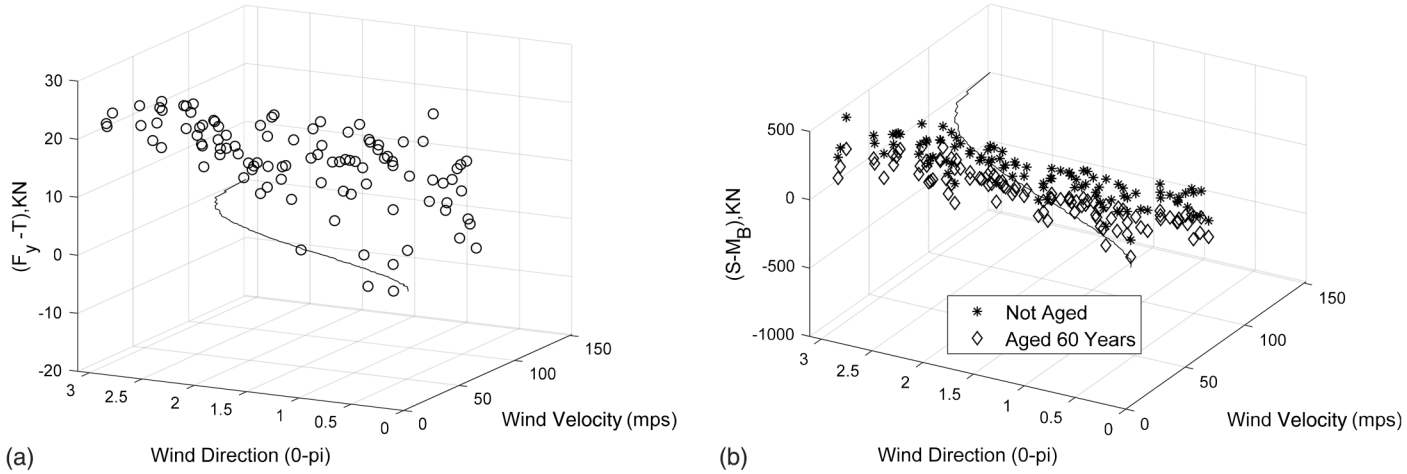


**Fig. 4.** Sampled response surface subjected to Hurricane Category III for (a) conductors; and (b) generic poles further subject to aging.

defines the system robustness. Given a sample value from the space $\mathcal{A}$, $A_m$, the probability mass distribution (PMD) is denoted by $P_{AC}(\cdot)$, which has the following mathematical expression:

$$P_{AC}(A_m|H,G) = \begin{cases} (1-P_c)^N(1-P_w)^N, & \text{if } m=0 \\ (1-P_c)^{N-m}(1-P_w)^{N-m}(P_c+P_w-P_cP_w), & \text{if } 1 \le m < N \\ (P_c+P_w-P_cP_w), & \text{if } m=N \end{cases} \tag{7}$$

The appendix provides more details on the formulation, and an illustrative example is given to enhance the understanding. Note that when $m=0$ and $P_{ZL}=(1–P_c)^N\ (1–P_w)^N$, $P_{ZL}$ defines the conditional probability of so-called zero loss of ACs, which is essentially the reliability of the power-delivery system. On the other hand, when $m=N$ and $P_{TL}=P_c+P_w–P_cP_w$, $P_{TL}$ defines the probability of the maximal total loss of customers (i.e., $Q_{100}$). Now with the expression in Eq. (7) and the definition of $A_m$, the mean ACs, denoted by $Q(H,G)$, can be defined using the law of total expectation:

$$Q(H,G) = \sum_{A_m \in \mathcal{A}} A_m P_{AC}(A_m|H,G) \tag{8}$$

Eq. (8) defines the expectations of ACs, which can be treated as the variable mean of the dropped system functionality given the hurricane category $H$ and a certain aging factor $G$. Accordingly, the mean robustness of the system $Q_R$ is expressed as $Q_{100}–Q(H,G)$. Note that if desired, the variance of ACs can be calculated.

Fig. 5 illustrates the distribution plots based on Eq. (8) (defined over 100 randomly generated $A_m$ with $A_{100}=500$) given two analytical cases: Case 1 is a high-reliability system (assuming $P_c=1/500$, $P_w=1/200$), while Case 2 is a low-reliability system ($P_c=1/100$, $P_w=1/50$). Both cases use a randomly generated 100 different customers for 100 conductor-pole units (each unit serves from 1 to 10 customers). For Case 1, the system reliability $P_{ZL}$ is 49.6%, whereas in Case 2, $P_{ZL}=4.9\%$. One can further see that, as predicted by Eq. (1), for the low-reliability system, although the probability of losing the least number of customers (i.e., $A_1$ served by the ending power-conductor unit) is smaller, the probabilities of losing a higher number of customers increase much faster than in the high-reliability system owing to the cascading effect. As a result, using the $A_m$ set, the mean loss of the high-reliability system is 157.4 customers, whereas the low-reliability system is 386.2 customers. This is consistent with the understanding of either a low- or high-reliability system and its effects on system functionality.

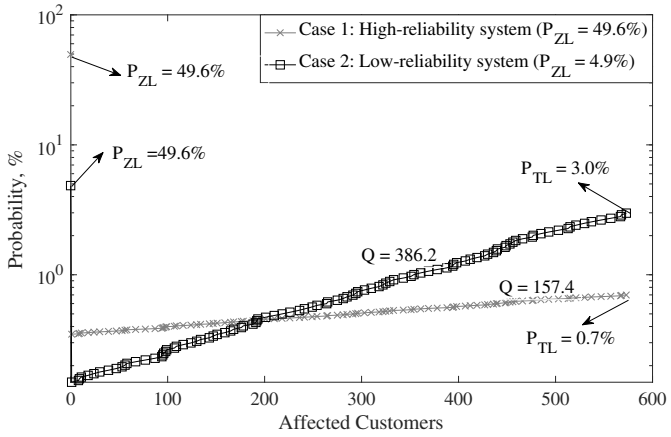


**Fig. 5.** Analytical distribution function of affected customers.

### Probabilistic System Recovery Modeling

A concept of variable restoration time for civil-infrastructure components has been proposed in the literature (Anghel et al. 2007; Ouyang et al. 2012). For example, the restoration time of any failed component by repair or replacement is taken as the summation of two random time variables $a$ and $b$ (e.g., $a$ takes a uniform distribution and $b$ an exponential distribution). In this paper, a general and analytical restoration-time modeling approach for power-delivery components is proposed (which are different from the system-level recovery function to be introduced later). The significant differentiation of this approach from previous efforts is the inclusion of two parameters that account for local resourcefulness and spatial distribution.

First, the authors state that local resources for the component-level restoration affect the system-level recovery rate and the resulting recovery function as well. Quantification of available resources within the system is a crucial task for selecting the component restoration function. However, it is challenging to characterize local resourcefulness since it spans multiple resilience dimensions (social, organizational, behavioral, and technological) (Bruneau et al. 2003). In addition, if failure occurs within more than two local power-delivery systems, local competition and cooperation are expected in resource allocation, which further complicates component restoration and system recovery. Without addressing such local competition and cooperation, a simplified modeling approach may be developed in terms of a weighting variable from each of the resilience dimensions (Zona et al. 2020). Owing to the scope of this framework-based paper, such a possibility is not discussed here; rather, a globally lumped and static resourcefulness index $\kappa$ is adopted. In this study, the authors introduce a global variable, referred to as a resourcefulness variable and denoted by $\kappa$, which ranges from 0 to 1, where 0 indicates a complete lack of resources and 1 maximally adequate resources.

The other variable that affects the restoration of a component is the geospatial location of the component coupled with the dynamic availability of resources. Specifically, for a rural power-delivery system, this distance is taken as the relative distance from the substation to a remote pole or cable, assuming that the restoration time increases monotonically as this relative distance increases. In this paper, considering a pole or a cable at the $i$th unit that potentially fails, $D_i$ denotes the geospatial distance at this component. In practical implementation, one may further consider local terrain or other geospatial challenging factors when calculating $D_i$ values. In this paper, a simple two-dimensional Euclidean distance metric is used to calculate $D_i$.

With the definitions of $\kappa$ and $D_i$, a general component restoration model is proposed in Eq. (9):

$$R(i) = r_0 \times e^{\lambda_1 \times Di} \times e^{\lambda_2(1-\kappa)} \tag{9}$$

This restoration model assumes that the restoration time for a generic pole or a conductor cable decreases exponentially as the distance to the substation ($D_i$) increases and increases exponentially as the resourcefulness ($\kappa$) increases. In Eq. (9), $r_0$, $\lambda_1$ ($\lambda_1 > 0$), and $\lambda_2$ ($\lambda_2 > 0$) are empirical (user-defined), constant parameters. The constant $r_0$ is a user-determined parameter that approximates the expected hours for repairing the pole or conductor closest to the substation with the maximal resource. The constants $\lambda_1$ and $\lambda_2$ are parameters that incorporate other uncertainties such as flooded streets, traffic blockade, and fallen trees, for example, that could interrupt the restoration. In this paper, an empirical procedure is used to estimate $\lambda_1$ and $\lambda_2$ and is detailed in the numerical experiment later. When the restoration times for the $i$th pole and cable are calculated, they are denoted by $Rw(i)$ and $Rc(i)$, respectively.

With $Rw(i)$, $Rc(i)$, and the PMF, $P_{AC}(A_m|H,G)$, the mean restoration time of the system considering all components at $A_m$ is determined, denoted by $T_{\text{sys}}$. As shown by Eq. (10), it is a mathematical expectation of the restoring times for all the possible combinations of the failed poles and conductors and the successful ones, conditional on the event of $A_m$. The appendix provides the key steps to obtain this expression:

$$T_{sys}(A_m) = \begin{cases} 0, & \text{if } m = 0 \\ \dfrac{P_c \times Rc(m) + P_w \times Rw(m)}{P_c + P_w - P_c P_w}, & \text{if } m = 1 \\ P_c\left(\displaystyle\sum_{i=1}^{m-1} Rc(m) + \frac{Rc(m)}{P_c + P_w - P_c P_w}\right) + P_w\left(\sum_{i=1}^{m-1} Rw(m) + \frac{Rw(m)}{P_c + P_w - P_c P_w}\right), & \text{if } 1 < \text{if } m \le N \end{cases} \tag{10}$$

Given this function, the total mean restoration time considering the distribution of all failure events and the component restoration times can be further obtained based on the law of total expectation:

$$T^t_{sys} = \sum_{m=0}^{N} T_{sys}(Am) P_{AC}(A_m|H,G) = \ \ldots$$
$$= P_c \sum_{m=1}^{N} Rc(m) + P_w \sum_{m=1}^{N} Rw(m) \tag{11}$$

which can be used a scalar measure of the total restoration time cost. Eq. (11) also indicates that if the whole linear power-delivery system is considered, the total mean restoration time is simply the sum of the total restoration time of all poles and of all conductors weighted by the probability of failure of a generic pole and a conductor, respectively. Subsequently, the variance of the total restoration time and the coefficient of variation (denoted by $\text{COV}_\text{T}$) can be calculated using Eqs. (12) and (13), respectively:

$$\sigma_T^2 = \sum_{m=0}^{N} [T^t_{sys} - T_{sys}(A_m)]^2 P_{AC}(A_m|H,G) \tag{12}$$

$$\text{COV}_\text{T} = \frac{\sigma_T}{T^t_{sys}} \times 100\% \tag{13}$$

### Probabilistic Resilience Modeling

The probabilistic resilience model is the final step of the proposed analytical framework. As discussed, the system recovery function is key to measuring resilience. Unlike the restoration time for a component or a system, a system recovery function is a continuous model that can measure the rate of recovery. However, the rate of recovery poses a very challenging problem mathematically. In the literature (e.g., Cimellaro et al. 2010), three canonical forms, linear, exponential, and trigonometric, are expressed as follows:

$$\text{Linear: } f_{rec}(t) = \frac{(Q_{100} - Q_R)(t - t_{oe})}{T^t_{sys}} + Q_R \tag{14}$$

$$\text{Trigonometric: } f_{rec}(t) = (Q_{100} - Q_R)\left(1 - \cos\left(\frac{\pi(t - t_{oe})}{2T^t_{sys}}\right)\right) + Q_R \tag{15}$$

$$\text{Exponential: } f_{rec}(t) = \gamma(exp^{\frac{t-t_{oe}}{T^t_{sys}}}) + Q_R - \gamma \tag{16}$$

where $Q_{100}$ = full functionality of system before strike; $Q_R$ = residual functionality after strike; $t_{oe}$ = time of strike; and $\gamma = (Q_{100} - Q_R)/(e-1)$. Given Eqs. (14)–(16), choosing a recovery function is highly empirical and is regarded as a higher-level decision-making process; that is, it is determined by the stakeholders in the power system. In general, the trigonometric recovery function is more realistic, demonstrating an initially slow-paced recovery rate, then a fast rate in the later phase. Nonetheless, if the resourcefulness is very high (e.g., $\kappa = 0.9$), one may proceed with the exponential function. When no knowledge about the recovery rate exists or the resourcefulness is considered low, the linear recovery function may be preferred.

Hence, given a select system recovery function ($f_{rec}$), the controlling period ($T_C$), and the mean restoration time at $A_m$ or $T_{\text{sys}}(A_m)$, the mean system resilience (MSR) given a failure event $A_m$, denoted by $R_{sys}(A_m)$, is computed using Eq. (1) over the time interval $[t_{oe},\ t_c]$. From the calculated resilience measurements $R_{sys}(A_m)$, TMSR is further computed using the law of total expectation:

$$R^t_{sys} = \sum_{m=1}^{N} R_{sys}(A_m) P_{AC}(A_m|H,G) \tag{17}$$

Note that both MSR and TMSR defined herein are still retrospectively conditional on the hurricane category $H$ and the aging factor $G$. As similarly expressed previously, the variance for the total system resilience can be calculated as follows:

$\sigma_R^2 = \sum_{m=1}^{N} [(R_{sys}^t - R_{sys}(A_m)]^2 P_{AC}(A_m|H, G)$. The coefficient of variation for the total system resilience, denoted by $\mathrm{COV_R} = \sigma_R / R_{sys}^t \times 100\%$, can be used to measure the variability of the total system resilience.

## Numerical Example

### System Configuration and Parameters

Given the simplified configuration in Fig. 2(a), it is assumed that one transmission line with a voltage level of 450 KV runs in the middle of the area. This transmission line passes through the substation where the voltage level steps down to a distribution level of 15 KV. From the substation, three-phase feeder (primary) lines (each 15 KV) emanate radially for rural distribution. These primary feeder lines are assumed to have an American Wire Gauge (AWG) 4/0 , i.e., 25.4 mm (0.53 in.) diameter without insulation, which is commonly found in rural distribution systems. The average total length considered for a feeder line is 7.24 km (4.5 mi) with timber poles [Southern pine, Class 3, average diameter 0.24 m (9.5 in.) with a height of 7.93 m (26 ft) above and 2.74 m (9 ft) below ground, respectively] at a distance of 76.2 m (250 ft). As a result, a total of 95 poles (and 95 spans) are considered. These primary lines are branched off at the transverse direction to smaller three-phase secondary conductors (300 kcmil cu, 16.51 mm diameter) with insulation and then into single-phase laterals, which finally deliver power to local residences. For a linear power-delivery system, the total number of customers is assumed to be 400, which is randomly distributed to the $N$ conductor-pole units ($N = 95$).

### System Vulnerability and Function Calculation

A MATLAB version R2018a program was written that implements the proposed framework in this paper.

With the stochastic sampling described previously, the variable hurricane categories, the aging factor ($G = 5$, 20, 30, 60, and 90 years; and $G = 5$ years is considered as a nonaged condition). Figs. 6(a and b) show the failure probability curves for a generic conductor and a wood pole, respectively.

The PMF ($P_{AC}$) defined upon the sample space of ACs given a hurricane category of III and three different aging factors ($G = 5$, 20, and 60 years) is shown in Fig. 7. With the relatively high failure probabilities for the poles and the conductors (e.g., $Pc \approx 0.0853$, and $Pw \approx 0.2$ for nonaged poles; both Category III hurricanes), the probabilities at a small number of ACs are very small; then they increase rapidly as $A_m$ reaches the total number of customers ($Q_{100}$). Using Eq. (8), the expected mean ACs are obtained as 382, 385, and 390 customers, for $G = 5$, 20, and 60 years, respectively, at Category III hurricane. These mean loss values of ACs are consistent with the aging factors.

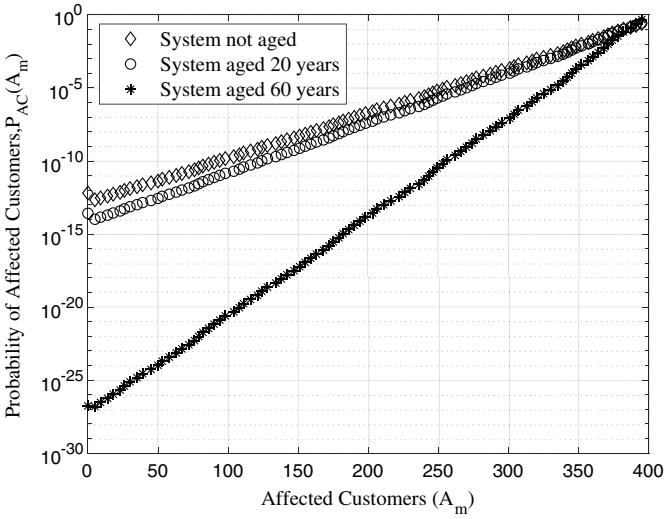


**Fig. 7.** Probability distribution of affected customers with different aging parameters.

### Component Restoration and System Recovery Calculation

To proceed with the recovery time and resilience calculation, an empirical parameterization procedure is adopted in this paper, which is summarized in the following steps:

1. The minimal hours for repairing a wood pole ($r_0^w$) and a conductor ($r_0^c$) are set as 5 and 3 h, respectively, which were similarly used in Ouyang et al. (2012).
2. Considering the instance of a pole, the constants $\lambda_1^w$ and $\lambda_2^w$ in Eq. (9) are estimated by assuming two empirical conditions. First, it is assumed that the maximal restoration times occur at the remotest component, namely, at the end pole, where $D_{95} =$ 7,242 m (4.5 mi). Taking the first condition, two different maximal restoration times occur at these two extreme resourcefulness conditions, namely, $\kappa = 0$ and $\kappa = 1$. In this paper, for the numerical experiment, the authors consider $R_w(95) = 20$ h with

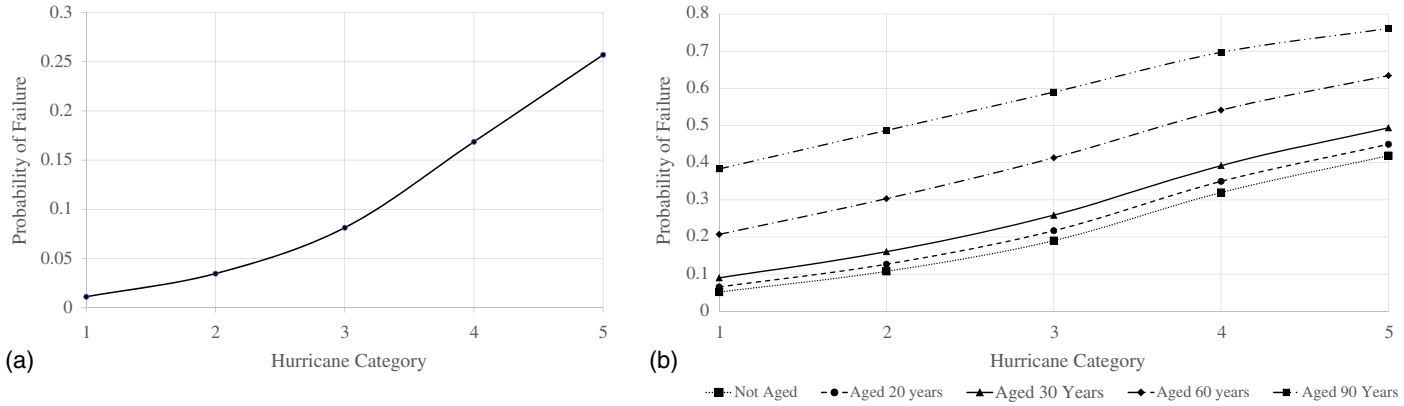


**Fig. 6.** Probability of failure as a function of hurricane category for (a) conductors; and (b) poles further subject to aging parameters.

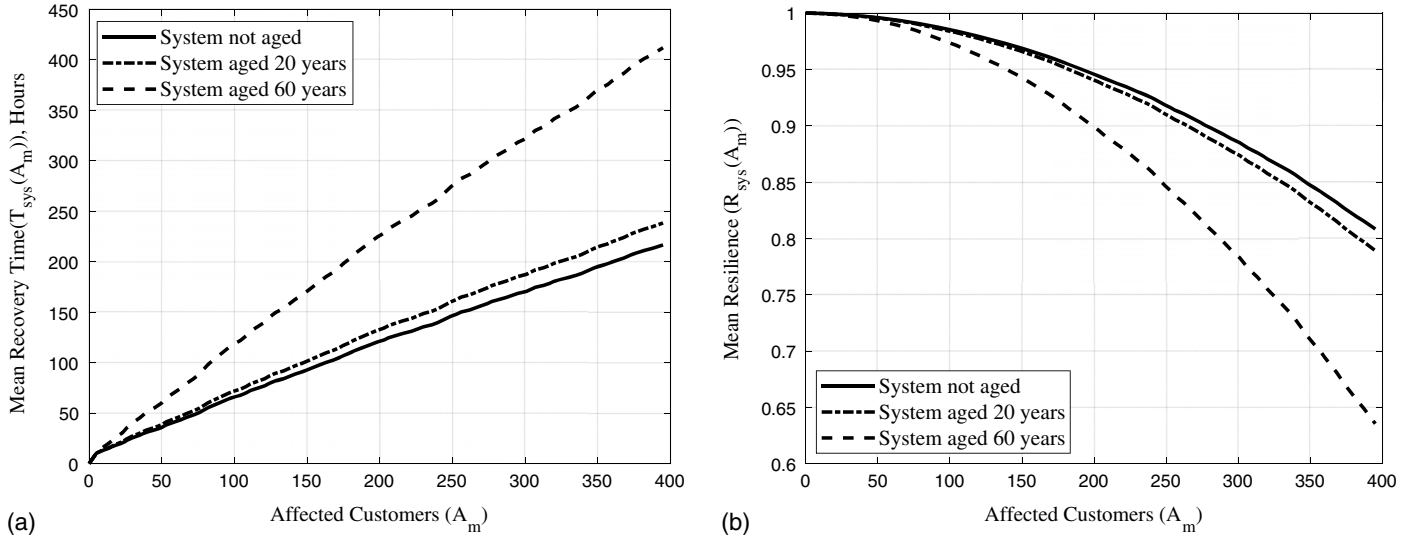


**Fig. 8.** (a) Mean recovery time; and (b) mean system resilience.

$\kappa = 0$, and $R_w(95) = 7$ h with $\kappa = 1$. By applying these two results to Eq. (9), the two restoration constants are solved, which yields $\lambda_1^w = 1.416 \times 10^{-5}$ and $\lambda_2^w = 1.05$.

3. Similarly, for the restoration time for a conductor, by repeating the previous step, except considering $Rc(95) = 18$ h with $\kappa = 0$ and $Rc(95) = 6$ h with $\kappa = 1$, the resulting restoration constants are solved as well: $\lambda_1^c = 2.917 \times 10^{-5}$ and $\lambda_2^c = 1.099$.
4. With this empirical and simplified procedure, the two restoration functions are obtained: $Rw(i) = 5e^{0.00001416 \times Di} e^{1.05(1-\kappa)}$ and $Rc(i) = 3e^{0.00002917 \times Di} e^{1.099(1-\kappa)}$.

By choosing a moderate-level resourcefulness value, in this example, $\kappa = 0.65$, the distribution of the mean system recovery time as a function of the ACs ($A_m$), or $T_{sys}(A_m)$, is shown in Fig. 8(a), where three aging conditions ($G = 5$, 20, and 60 years) are considered (given a Category III hurricane). The total mean recovery times and their variabilities for the different cases are computed based on Eqs. (11)–(13), which are $T_{sys}^t$ = 213.14, 235.22, and 411.73 h with $\text{COV}_T = 20.4\%$, 18.44%, and 10.42% for $G = 5$, 20, and 60 years, respectively.

### Resilience Calculation

Following the earlier description, the MSR of the system as a function of a customer loss event, or $R_{sys}(A_m)$, can be obtained. With the illustration in Fig. 8(a), $R_{sys}(A_m)$ is plotted in Fig. 8(b) considering three aging factors. In particular, considering the resourcefulness parameter of $\kappa = 0.65$, the trigonometric recovery function [Eq. (15)] is used in the resilience calculation. Note that aging factors adversely affect the system resilience at different levels of functionality losses in terms of the ACs. In particular, when the aging is taken as 60 years, the system resilience decreases significantly at all levels of function losses.

Eq. (17) provides the expression of the TMSR, which yields a scalar-value statistic that characterizes the system resilience. In addition, this TMSR measure can be used to evaluate the effects of resourcefulness. Three lower- to higher-level resourcefulness values are considered to compute TMSRs ($\kappa = 0.1$, 0.65, and 0.9). With $\kappa = 0.1$ and 0.65, the trigonometric recovery function is used too (however, the mean recovery time costs are different from the case of $\kappa = 0.65$). With a very high resourcefulness value ($\kappa = 0.95$), besides changing the mean restoration times and their distribution, it affects the selection of the system recovery function. In this case, the exponential function in Eq. (16) is used. Table 2 reports all the TMSR measurements, and Table 3 reports the $\text{COV}_R$ considering the parameter matrix of the aging factor ($G = 5$, 20, and 60 years) and the hurricane categories ($H = 1$, 2, 3, 4, and 5) for resourcefulness values of 0.1, 0.65, and 0.95, respectively. Fig. 9 partially summarizes the results in Table 2 by graphing the variations of TMSRs against the hurricane categories with a moderate aging value, $G = 20$. It is observed that within the same system with the same control period, the resilience can be very small (e.g., under $G =$ 20 years and $\kappa = 0.1$, TMSR = 0.3696 at $H =$ IV, and 0.1409 at $H =$ V), yet they increase significantly when the resourcefulness increases. Under the same $G$ and with $\kappa = 0.65$, TMSR increases to 0.6489 and 0.5221, respectively. Fig. 9 confirms this trend as well. This change in resilience thus proves the importance of

**Table 2.** Total mean system resilience at different resourcefulness and hurricane category levels

| Hurricane category | Resourcefulness | | |
|---|---|---|---|
| | $\kappa = 0.1$ | $\kappa = 0.65$ | $\kappa = 0.95$ |
| I | (0.9311, 0.9137, 0.7310)[a] | (0.9615, 0.9517, 0.8492) | (0.9744, 0.9679. 0.8994) |
| II | (0.8334, 0.8085, 0.5801) | (0.9070, 0.8930, 0.7649) | (0.9382, 0.9288. 0.8433) |
| III | (0.6744, 0.6397, 0.3619) | (0.8185, 0.7991, 0.0.6431) | (0.8794, 0.8664, 0.7624) |
| IV | (0.4085, 0.3696, 0.1207) | (0.6707, 0.6489, 0.5092) | (0.7813, 0.7668, 0.6736) |
| V | (0.1806, 0.1409,–0.0988[b]) | (0.5443, 0.5221, 0.3875) | (0.6975, 0.6827, 0.5929) |

[a]The three numbers from the left provide the estimation of TMSRs at 5, 20, and 60 years.
[b]The negative value herein is due to the fact that the calculated $T_{sys}$ is longer than the assumed $Tc$; to avoid a negative resilience value, a larger $Tc$ can be used.

**Table 3.** Coefficient of variations (%) for total system resilience at different resourcefulness and hurricane category levels

| Hurricane category | Resourcefulness | | |
|---|---|---|---|
| | $\kappa = 0.1$ | $\kappa = 0.65$ | $\kappa = 0.95$ |
| I | (6.35, 6.75, 2.77)[a] | (1.09, 1.15, 1.34) | (0.71, 0.75, 0.84) |
| II | (2.43, 2.53, 3.40) | (1.25, 1.27, 1.43) | (0.81, 0.82, 0.87) |
| III | (3.00, 3.17, 5.1) | (1.39, 1.43, 1.63) | (0.85, 0.86, 0.9) |
| IV | (4.77, 16.46, 13.87) | (1.94, 1.61, 1.76) | (0.94, 0.92, 0.93) |
| V | (10.05, 12.69, 15.35) | (1.84, 5.75, 2.16) | (0.96, 0.96, 0.94) |

[a]The three numbers in the parenthesis, e.g., 6.35, 6.75, 2.77, provide the COVs at the 5, 20, and 60 years, respectively.

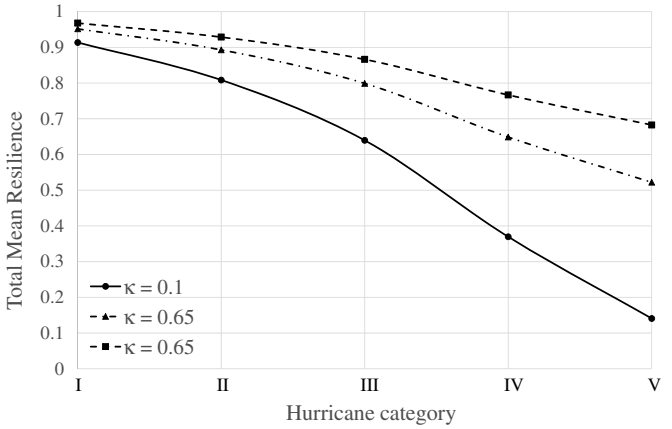


**Fig. 9.** Total mean system resilience at different hurricane levels and resourcefulness levels.

incorporating a resourcefulness parameter to quantify system resilience. When the variability of the measure of the total system resilience is considered, as shown in Table 3, it is observed that in general the hurricane category increases the variability, whereas the level of resourcefulness decreases the variability.

## Conclusions and Remarks

By focusing on power-delivery systems typically found in rural areas, this paper proposes a probabilistic framework for measuring the resilience of such systems. The framework starts with an order-reduced mechanics-based modeling approach that yields the conditional failure probability for wood poles and conductors. The remaining steps are fully mathematically tractable with closed-form formulations. First, the system functionality probability is defined on the event space of ACs. Second, a component-level restoration model is proposed, and the mean restoration time cost is formulated probabilistically considering the cascading effects. Finally, the mean resilience distribution and the total-system mean-resilience of the system are both formulated, the latter of which yields a scalar measure for linear power-delivery systems in rural areas. A numerical example is provided with realistic aging-related material degrading effects and considering different categories of hurricane winds. The resulting probabilistic distribution of ACs, restoration times, and system resilience are calculated using the proposed framework. The plots of the mean system resilience subject to different aging factors and the TMSR subject to the resourcefulness parameters insightfully demonstrate the effects of aging and local resourcefulness, one in the physical dimension and the other in the socioeconomic dimension.

Unlike the previous framework in the literature, the methodology provided in this paper provides a basis for probabilistically characterizing the system vulnerability and resilience at a local level (i.e., one linear power-delivery system that may span many miles in the US). This framework can be used to quantitatively assess system- or network-level resilience, which may alter the fact that to this end, often empirical models are used in network-based power-system-resilience assessment. It is further remarked that the proposed framework can be directly used for modeling a rural distribution system (with multiple radial distribution systems). In this situation, no system redundancy is found, and the proposed framework can be separately applied to each independent linear power-distribution subsystem. Note that in some large rural areas with clustered residential units or commercial assets, multiple local substations exist that allow for the adoption of power switches to provide alternative electricity feeding or system redundancy in case of a failure event. In this case, there exists an optimal condition for expressing the resilience at the system level; or more generally, there could be a resilience interval due to the possible combination of binary switches subject to extreme events. This optimization problem is beyond the scope of this paper. Nonetheless, the analytical framework presented in this paper provides the basis for computing the resilience of a local linear subsystem as a "node" in a complex system network with integer variables.

## Appendix. Mathematical Formulation of $P_{AC}$ and $T_{sys}$

Considering the power-delivery system in Fig. 2(b) that has $N$ poles and $N$ conductors in series, the state of a conductor or a pole is treated as binary: $s$ is for a conductor and $t$ for a pole, and $s = 1$ or $t = 1$ denotes failure (0 for success). Then the possible states of a conductor-pole unit form a set of 2-tuple binary state pairs: {(1, 1), (1, 0), (0, 1), (0, 0)}. Achieving the production of $A_m$ ACs is equivalent to this system state: (1) from the unit $N$ to the unit $(m + 1)$, all units need to be in the success state, each leading to a probability measure $(1 - Pc)\,(1 - Pw)$; (2) at the $m$th unit, the unit is in a state $\{(s, t)|(1 - s)(1 - t) \neq 1\}$ to create a cascading effect of losing $A_m$ customers, which includes all unit states except (0, 0) and leads to the probability measure $(Pc + Pw–PcPw)$ from the summation of the probabilities of the three unit states; and (3) from the unit $(m - 1)$ to the unit 1 (the end unit), the units can take any of a possible four unit states, which gives a total probability measure (i.e., 1) from the summation of $4^{m-1}$ different combinations of the unit states. The probability of this system state for ensuring the event $A_m$ gives rise to the mass probability $P_{AC}(A_m) = [(1-Pc)^{N-m}(1 - Pw)^{N-m}] \times (Pc + Pw–PcPw) \times 1$. Eq. (7) further elaborates this expression by defining the special cases at $m = 1$ and $m = N$.

To calculate the restoration time cost for a linear power-delivery system, one needs to consider separately the restoration time of all possible system states. By combination, given an event $A_m$, it is equivalent to a total number of $3 \times 4^{m-1}$ system states, each of which corresponds to a different total restoration cost. For each such system state, the mass probability is a joint function and can be defined as $P(A_m, F_m)$, where $F_m$ is a function of $\mathcal{B} = \{(s_i, t_i)|i = m, m - 1, \ldots, 1\}$, which defines one specific scenario of the system state from the $m$th to the first conductor-pole unit. This joint probability is expressed as

$$P[A_m, F_m(\mathcal{B})] = (1-P_c)^{N-m}(1-P_w)^{N-m}P_c^{s_m}(1-P_c)^{1-s_m}P_w^{t_m} \times (1-P_w)^{1-t_m}\ldots\prod_{i=1}^{m-1}P_c^{s_i}(1-P_c)^{1-s_i}P_w^{t_i}(1-P_w)^{1-t_i}$$

where $\{(s_m, t_m)|(1-s_m)(1-t_m) \neq 1\}$ still holds for the $m$th unit and $(s_i, t_i)$ takes any of the four binary state pairs. In this system state, the system restoration time is a summation of the individual time cost for each failed pole and conductor. Considering Eq. (9) and defining the restoration cost at the $i$th pole and conductor as $Rw(i)$ and $Rc(i)$, respectively, the total restoration $r[F_m(\mathcal{B})]$ is expressed as

$$r[F_m(\mathcal{B})] = \sum_{i=1}^{m} Rc(i)s_i + Rw(i)t_i$$

Given the two foregoing expressions, one can formulate the distribution of the mean restoration time conditional on the event $A_m$, defined as

$$T_{sys}(A_m) = \mathbf{E}[r(F_m(\mathcal{B}))|A_m] = \frac{\sum_{\mathcal{B}} r(F_m)P(A_m, F_m(\mathcal{B}))}{P(A_m)}$$
$$= P_c\left(\sum_{i=1}^{m-1} Rc(m) + \frac{Rc(m)}{P_c + P_w - P_cP_w}\right)$$
$$+ P_w\left(\sum_{i=1}^{m-1} Rw(m) + \frac{Rw(m)}{P_c + P_w - P_cP_w}\right)$$

Note that to obtain the result presented earlier [Eq. (10)], a mathematical induction method is recommended for handling the $\mathcal{B}$ set (i.e., by formulating the expression at $m = 1, 2, \ldots, m = k$ and then inducing it at $m = k + 1$). Given $T_{sys}(A_m)$, the total mean restoration time can be further obtained using the law of total expectation. Similarly, the distribution of mean system resilience can be subsequently obtained by applying Eq. (1) and $T_{sys}(A_m)$, and the TMSR as well by the law of total expectation.

## Data Availability Statement

Some or all data, models, or code generated or used during the study are available from the corresponding author by request. These include all the MATLAB programs and codes used to compute and generate and plot the tables and figures in this paper.

## References


Anghel, M., K. A. Werley, and A. E. Motter. 2007. "Stochastic model for power grid dynamics." In *Proc., 2007 40th Annual Hawaii Int. Conf. on System Sciences (HICSS'07)*, 113. New York: IEEE.

ANSI (American National Standards Institute). 2017. *Wood poles: Specifications and dimensions*. ANSI O5.1. New York: ANSI.

Archer, C. L., and M. Z. Jacobson. 2003. "Spatial and temporal distributions of U.S. winds and wind power at 80 m derived from measurements." *J. Geophys. Res. Atmos.* 108 (D9). https://doi.org/10.1029/2002JD002076.

Ayyub, B. M. 2014. "Systems resilience for multihazard environments: Definition, metrics, and valuation for decision making." *Risk Anal.* 34 (2): 340–355. https://doi.org/10.1111/risa.12093.

Bier, V. M., E. R. Gratz, N. J. Haphuriwat, W. Magua, and K. R. Wierzbicki. 2007. "Methodology for identifying near-optimal interdiction strategies for a power transmission system." *Reliab. Eng. Syst. Saf.* 92 (9): 1155–1161. https://doi.org/10.1016/j.ress.2006.08.007.

Bilal, A. M. 2015. "Practical resilience metrics for planning, design, and decision making." *ASCE-ASME J. Risk Uncertainty Eng. Syst. A: Civ. Eng.* 1 (3): 04015008. https://doi.org/10.1061/AJRUA6.0000826.

Bilal, A. M., and K.-L. Lai. 1990. "Structural reliability assessment using Latin hypercube sampling." In *Proc., 5th Int. Conf. on Structural Safety and Reliability 1989 (ICOSSAR'89)*, 1177–1184. New York: ASCE.

Brennan, M. A., and C. G. Flint. 2007. "Uncovering the hidden dimensions of rural disaster mitigation: Capacity building through community emergency response teams." *South. Rural Sociol.* 22 (2): 111–126.

Britt, E. 2017. "Hurricanes Harvey and Irma: Electric industry impacts, restoration, and cost recovery." Infrastructure Accessed June 1, 2019. http://www.dwmrlaw.com/wp-content/uploads/2018/04/ABA_INFRA57-1.pdf.

Brown, R. E., and H. L. Willis. 2006. "The economics of aging infrastructure." *IEEE Power Energy Mag.* 4 (3): 36–43. https://doi.org/10.1109/MPAE.2006.1632452.

Bruneau, M., S. E. Chang, R. T. Eguchi, G. C. Lee, T. D. O'Rourke, A. M. Reinhorn, M. Shinozuka, K. Tierney, W. A. Wallace, and D. Von Winterfeldt. 2003. "A framework to quantitatively assess and enhance the seismic resilience of communities." *Earthquake Spectra* 19 (4): 733–752. https://doi.org/10.1193/1.1623497.

Burbank, K., T. Davison, S. Saifee, G. WHite, C. Beck, and D. Quan. 2005. "An estimate of lost earnings due to electric supply disruption." In *The case of Florida's 2004 hurricane season*. Orlando, FL: FEMA.

Carlos Agustín, E.-S. 2013. "Estimation of extreme wind speeds by using mixed distributions." *Ingeniería, Investigación y Tecnología* 14 (2): 153–162. https://doi.org/10.1016/S1405-7743(13)72233-9.

Chen, C., J. Wang, F. Qiu, and D. Zhao. 2016. "Resilient distribution system by microgrids formation after natural disasters." *IEEE Trans. Smart Grid* 7 (2): 958–966. https://doi.org/10.1109/TSG.2015.2429653.

Cimellaro, G. P., A. M. Reinhorn, and M. Bruneau. 2010. "Framework for analytical quantification of disaster resilience." *Eng. Struct.* 32 (11): 3639–3649. https://doi.org/10.1016/j.engstruct.2010.08.008.

Dagher, H. J. 2006. *Reliability-based design of utility pole structures*. Reston, VA: ASCE.

Danica Coto. 2018. "Lights slowly come on for Puerto Ricans in rural areas." Accessed June 1, 2019. https://www.csmonitor.com/USA/2018/0716/Lights-slowly-come-on-for-Puerto-Ricans-in-rural-areas.

Davidson, R. A., H. Liu, I. K. Sarpong, P. Sparks, and D. V. Rosowsky. 2003. "Electric power distribution system performance in Carolina hurricanes." *Nat. Hazard. Rev.* 4 (1): 36–45. https://doi.org/10.1061/(ASCE)1527-6988(2003)4:1(36).

DHS (Department of Homeland Security). 2011. *Presidential policy directive/PPD-8: National preparedness*. Washington, DC: DHS.

Dueñas-Osorio, L., J. I. Craig, B. J. Goodno, and A. Bostrom. 2007. "Interdependent response of networked systems." *J. Infrastruct. Syst.* 13 (3): 185–194. https://doi.org/10.1061/(ASCE)1076-0342(2007)13:3(185).

Edwards, P., and R. B. Hurst. 2001. "Level-crossing statistics of the horizontal wind speed in the planetary surface boundary layer." *Interdiscip. J. Nonlinear Sci.* 11 (3): 611–618. https://doi.org/10.1063/1.1379310.

Espinoza, S., M. Panteli, P. Mancarella, and H. Rudnick. 2016. "Multi-phase assessment and adaptation of power systems resilience to natural hazards." *Electr. Power Syst. Res.* 136 (Jul): 352–361. https://doi.org/10.1016/j.epsr.2016.03.019.

Gao, H., Y. Chen, Y. Xu, and C. Liu. 2016. "Resilience-oriented critical load restoration using microgrids in distribution systems." *IEEE Trans. Smart Grid* 7 (6): 2837–2848. https://doi.org/10.1109/TSG.2016.2550625.

Gascó-Hernandez, M., M. Zheleva, P. Bogdanov, and J. R. Gil-Garcia. 2019. "Towards a socio-technical framework for bridging the digital divide in rural emergency preparedness and response: Integrating user adoption, heterogeneous wide-area networks, and advanced data science." In *Proc., 20th Annual Int. Conf. on Digital Government Research, Mohamed bin Rashid School of Government*, 362–369. New York: Association for Computing Machinery.

Guikema, S. D., and J. P. Goffelt. 2008. "A flexible count data regression model for risk analysis." *Risk Anal.* 28 (1): 213–223. https://doi.org/10.1111/j.1539-6924.2008.01014.x.

Impollonia, N., G. Ricciardi, and F. Saitta. 2011. "Statics of elastic cables under 3D point forces." *Int. J. Solids Struct.* 48 (9): 1268–1276. https://doi.org/10.1016/j.ijsolstr.2011.01.007.

Kapucu, N., C. V. Hawkins, and F. I. Rivera. 2013. "Disaster preparedness and resilience for rural communities." *Risk Hazard. Crisis Public Policy* 4 (4): 215–233. https://doi.org/10.1002/rhc3.12043.

Kenward, A., and U. Raja. 2014. "Blackout: Extreme weather, climate change and power outages." Accessed June 1, 2019. https://assets.climatecentral.org/pdfs/PowerOutages.pdf.

Kwasinski, A. 2016. "Quantitative model and metrics of electrical grids' resilience evaluated at a power distribution level." *Energies* 9 (2): 93. https://doi.org/10.3390/en9020093.

Li, J., X. Ma, C. Liu, and K. P. Schneider. 2014. "Distribution system restoration with microgrids using spanning tree search." *IEEE Trans. Power Syst.* 29 (6): 3021–3029. https://doi.org/10.1109/TPWRS.2014.2312424.

Liu, H., R. A. Davidson, D. V. Rosowsky, and J. R. Stedinger. 2005. "Negative binomial regression of electric power outages in hurricanes." *J. Infrastruct. Syst.* 11 (4): 258–267. https://doi.org/10.1061/(ASCE)1076-0342(2005)11:4(258).

Morrell, J. J. 2012. *Wood pole maintenance manual: 2012 edition, research contribution 51*. Corvallis, OR: Forest Research Laboratory, Oregon State Univ.

Ouyang, M., and L. Dueñas-Osorio. 2014. "Multi-dimensional hurricane resilience assessment of electric power systems." *Struct. Saf.* 48 (May): 15–24. https://doi.org/10.1016/j.strusafe.2014.01.001.

Ouyang, M., L. Dueñas-Osorio, and X. Min. 2012. "A three-stage resilience analysis framework for urban infrastructure systems." *Struct. Saf.* 36–37 (May): 23–31. https://doi.org/10.1016/j.strusafe.2011.12.004.

Pang, W., Z. Chen, F. Liu, and R. Holmes. 2013. "Failure risk of 230 kV electricity transmission lines in South Carolina under hurricane wind hazards." In *Proc., ATC & SEI Conf. on Advances in Hurricane Engineering 2012*. Reston, VA: ASCE.

Panteli, M., and P. Mancarella. 2017. "Modeling and evaluating the resilience of critical electrical power infrastructure to extreme weather events." *IEEE Syst. J.* 11 (3): 1733–1742. https://doi.org/10.1109/JSYST.2015.2389272.

Panteli, M., C. Pickering, S. Wilkinson, R. Dawson, and P. Mancarella. 2017. "Power system resilience to extreme weather: Fragility modeling, probabilistic impact assessment, and adaptation measures." *IEEE Trans. Power Syst.* 32 (5): 3747–3757. https://doi.org/10.1109/TPWRS.2016.2641463.

Reed, D. A., K. C. Kapur, and R. D. Christie. 2009. "Methodology for assessing the resilience of networked infrastructure." *IEEE Syst. J.* 3 (2): 174–180. https://doi.org/10.1109/JSYST.2009.2017396.

Sakai, T., M. Nakajima, K. Tokaji, and N. Hasegawa. 1997. "Statistical distribution patterns in mechanical and fatigue properties of metallic materials." *Mater. Sci. Res. Int.* 3 (2): 63–74. https://doi.org/10.2472/jsms.46.6Appendix_63.

Southwire. 2013. *Bare copper wire and cable*. Carrollton, GA: Southwire Company.

Torrent, R. J. 1978. "The log-normal distribution: A better fitness for the results of mechanical testing of materials." *Matériaux et Constr.* 11 (4): 235–245. https://doi.org/10.1007/BF02551768.

Vivekanandan, N. 2012. "Comparison of estimators of extreme value distributions for wind data analysis." *Bonfring Int. J. Data Min.* 2 (3): 16–20. https://doi.org/10.9756/BIJDM.1503.

Vugrin, E. D., A. R. Castillo, and C. A. Silva-Monroy. 2017. "*Resilience metrics for the electric power system: A performance-based approach*. SAND2017-1493. Livermore, CA: Sandia National Laboratories.

Wang, C.-H., R. H. Leicester, and M. Nguyen. 2008. "Probabilistic procedure for design of untreated timber poles in-ground under attack of decay fungi." *Reliab. Eng. Syst. Saf.* 93 (3): 476–481. https://doi.org/10.1016/j.ress.2006.12.007.

Warwick, M., and M. Hoffman. 2016. *Electricity distribution system baseline report for DOE quadrennial energy review*. PNNL-25187. Richland, WA: Pacific Northwest National Laboratory.

Yao, Y., T. Edmunds, D. Papageorgiou, and R. Alvarez. 2007. "Trilevel optimization in power network defense." *IEEE Trans. Syst. Man Cybern. C (Appl. Rev.)* 37 (4): 712–718. https://doi.org/10.1109/TSMCC.2007.897487.

Yuan, H., W. Zhang, J. Zhu, and A. C. Bagtzoglou. 2018. "Resilience assessment of overhead power distribution systems under strong winds for hardening prioritization." *ASCE-ASME J. Risk Uncertainty Eng. Syst. A: Civ. Eng.* 4 (4): 04018037. https://doi.org/10.1061/AJRUA6.0000988.

Zhu, D., D. Cheng, R. P. Broadwater, and C. Scirbona. 2007. "Storm modeling for prediction of power distribution system outages." *Electr. Power Syst. Res.* 77 (8): 973–979. https://doi.org/10.1016/j.epsr.2006.08.020.

Zona, A., O. Kammouh, and G. P. Cimellaro. 2020. "Resourcefulness quantification approach for resilient communities and countries." *Int. J. Disaster Risk Reduct.* 46: 101509. https://doi.org/10.1016/j.ijdrr.2020.101509.